

Conclusion générale

Le travail présenté dans le cadre de cette thèse porte sur une étude expérimentale concernant des couches nanostructurées à base de Ni. Des dépôts Ni-P ont été réalisés par électrodéposition à partir d'un bain au sulfate du nickel, sodium hypophosphite, acide borique, chlorure de sodium et saccharine, en faisant varier le potentiel et le temps de déposition. Les caractérisations morphologique, structurale, microstructurale, mécanique, magnétique et électrochimique des dépôts Ni-P ont été faites par microscopie électronique à balayage, diffraction de rayons X en utilisant un programme d'affinement structural (MAUD) basé sur la méthode Rietveld, microduromètre, magnétomètre à échantillon vibrant et analyse potentiodynamique. Les principaux résultats obtenus se résument comme suit :

- 1- La morphologie des surfaces présente une structure dense, lisse et uniforme et est composé des petites particules dont la taille est égale 0,1 μm .
- 2- L'épaisseur des dépôts varie entre 734 et 971 μm selon l'irrégularité du dépôt.
- 3- La teneur en phosphore varie entre 8,64 at.% et 12,21 at.% en surface et entre 4,10 at.% et 6,7 at.% en volume. L'hétérogénéité chimique des dépôts peut être attribuée à la différence entre le potentiel de déposition du Ni et du P.
- 4- La structure des dépôts est constituée soit d'une solution solide Ni(P) avec deux structures cubique à faces centrées Ni(P)-1 et Ni(P)-2 dispersées dans une matrice amorphe, soit d'un mélange de Ni_2P , Ni(P)-1 et Ni(P)-2.
- 5- La concentration du phosphore introduit dans le réseau cristallin du nickel varie de 0,08 à 1,05 % et de 7,18 à 8,32 % pour les deux solutions solides Ni(P)-1 et Ni(P)-2, respectivement.
- 6- La taille des cristallites de la solution solide Ni(P)-1 est de l'ordre de 10 nm. Elle augmente de 98 nm pour le dépôt obtenu à -1V pendant 10 min.

- 7- La taille des cristallites de la solution solide Ni(P)-2 augmente avec l'évolution du potentiel de 93 à 100 nm dans les couches déposées pendant 10 min et de 51 à 89 nm dans les couches déposées pendant 20 min.
- 8- La proportion de la phase amorphe augmente avec l'évolution du potentiel appliqué pour atteindre une valeur de 26% dans la couche déposée à -1V pendant 20 min.
- 9- Les valeurs moyennes de la microdureté varient entre 128,4 et 665,4 $H_{V0,3}$. Elle augmente avec la diminution de la taille des cristallites de la solution solide Ni(P)-2.
- 10- La coercivité (H_c) mesurée en champ parallèle est plus élevée que celle obtenue lorsque le champ magnétique est perpendiculaire au plan.
- 11- La réduction de M_s peut être liée à la présence des atomes non magnétiques de phosphore dans le réseau cristallin du nickel.
- 12- Le dépôt obtenu à un potentiel de -1V pendant 20 min possède une meilleure résistance à la corrosion caractérisée par une résistance à la polarisation, R_p , de $1810 \Omega\text{cm}^2$, un potentiel de corrosion de -168 mV et un taux de porosité très faible (0,0002 %).

La variation du potentiel appliqué résulte en une augmentation de la proportion relative de la phase amorphe et une amélioration de la résistance de à corrosion, alors que la variation du temps de dépôt conduit à une augmentation de la taille des nodules, de la microdureté et de l'aimantation à saturation. Par conséquent, les couches déposées à -1V présentent les meilleures propriétés morphologiques, structurales, magnétiques et électrochimiques.

Comme perspectives, il serait intéressant d'étudier l'influence des paramètres de déposition sur la stabilité thermique de différents dépôts à base de nickel.

Microstructure and Magnetic Properties of NiP Alloys

**S. Alleg, A. Boussaha, W. Tebib,
M. Zergoug & J. J. Suñol**

**Journal of Superconductivity and
Novel Magnetism**
Incorporating Novel Magnetism

ISSN 1557-1939

J Supercond Nov Magn
DOI 10.1007/s10948-016-3397-2



Your article is protected by copyright and all rights are held exclusively by Springer Science +Business Media New York. This e-offprint is for personal use only and shall not be self-archived in electronic repositories. If you wish to self-archive your article, please use the accepted manuscript version for posting on your own website. You may further deposit the accepted manuscript version in any repository, provided it is only made publicly available 12 months after official publication or later and provided acknowledgement is given to the original source of publication and a link is inserted to the published article on Springer's website. The link must be accompanied by the following text: "The final publication is available at link.springer.com".

Microstructure and Magnetic Properties of NiP Alloys

S. Alleg¹ · A. Boussaha¹ · W. Tebib¹ · M. Zergoug² · J. J. Suñol³

Received: 8 November 2015 / Accepted: 6 January 2016
© Springer Science+Business Media New York 2016

Abstract Ni-P alloys were prepared by electrodeposition on a copper substrate at different plating conditions (applied potential and deposition time). The morphology, composition, microstructure, structure, and magnetic properties of the films were investigated by scanning electron microscopy, energy-dispersive spectrometry, X-ray diffraction, and vibrating sample magnetometry, respectively. The phosphorous content is about 8.6–12.2 at.%. The deposits exhibit either a nanocomposite structure where Ni(P)–1 and Ni(P)–2 solid solutions are embedded into an amorphous matrix, or a mixture of Ni₂P phosphide and Ni(P)–1 and Ni(P)–2 solid solutions. The coercivity and magnetization are plating condition dependent. All samples exhibit a soft magnetic character with coercivity lower than 58 Oe. The squareness ratio Mr/Ms values that are in the range 0.019–0.123 correspond to a multidomain (< 0.1) for all samples except sample B (–1.15 V, 10 min) which falls into a pseudo-single domain (Mr/Ms = 0.123).

Keywords Electrodeposition · Ni-P alloys · Microstructure · Magnetic properties · X-ray diffraction

1 Introduction

Electrodeposition has received much interest since it is an effective method to produce dense and thick deposits over a large surface area in a relatively short time by means of a simple process. It is also a low-temperature processing route to produce nanostructured materials. The increased interest in technology for electrodeposition is due to its low cost, versatility, high production rates, and industrial applicability [1–3].

Nickel-phosphorous (Ni-P) alloys have attracted many considerations owing to their good mechanical and chemical properties such as high hardness, high strength, high corrosion resistance, good wear resistance, solder ability, and uniformity of coating thickness [4]. Due to their high hardness, Ni-P alloys are suitable for diamond turning applications including fabrication of large optics and other high-precision parts [5]. Moreover, Ni-P coatings can be used as catalytic coatings for hydrogen evolution reactions [6], thin-film resistors, and under-layer in thin-film memory disks [7, 8]. The Ni-P system is very complex and exciting over a wide range of concentrations since the crystalline compounds Ni₁₂P₅, Ni₅P₂, Ni₂P, Ni₃P, NiP₂, and NiP have different structures which are P content dependent. Also, Ni₅P₂, Ni₂P, and Ni₃P phosphides have attracted much attention due to their excellent properties and potential applications such as corrosion-resistant, oxidation-resistant luminescent devices and electronic components [9]. It has been reported that nanocrystalline (NC) and amorphous phases with different P contents are formed and the average grain size decreases when the deposition content of P increases in the Ni matrix [10]. The amount of P in the Ni-P alloys influences the microstructure and the characteristics of the as-deposited films [11]. The transition from a crystalline to an amorphous structure takes place over a range

✉ S. Alleg
safia.alleg@yahoo.fr; safia.alleg@univ-annaba.dz

¹ LM2S, Department of Physics, Badji Mokhtar Annaba University, BP12, Annaba 23000, Algeria

² CSC, Route de Dely Brahim BP 64, Chéraga 16002, Algiers, Algeria

³ Department de Física, Universitat de Girona, Campus Montillivi, Girona 17071, Spain

of P concentrations rather than in an abrupt way at a certain composition [12–14]. The Ni-P alloys are generally classified into three categories: low P (2–7 at.%), medium P (8–18 at.%), and high P (more than 19 at.% P) [15, 16].

Amorphous and/or NC Ni-P alloys can be obtained by various methods such as electrodeposition, melt spinning, vapor deposition, chemical bath deposition, and ion implantation up to 42 at.% P. Electrodeposition is one of the most commonly used methods for preparing Ni-P alloys because the standard reduction potentials for Ni (−0.25 V) and P (−0.28 V) are near to each other. Hence, many metastable and amorphous phases have been reported since the first amorphous Ni-P alloys prepared by chemical bath deposition and electrodeposition [17]. Nonetheless, the intrinsic (short-/medium-range order) and extrinsic (preparation method, surface, impurities, etc.) non-homogeneities led to controversial results regarding the structure (saturated solid solution, NC, amorphous, or microcrystalline), magnetic, and electronic properties. Thus, despite a large number of research activities on the different aspects of electrodeposited Ni-P alloys, there is still a lack of information about the relationship between the plating parameters and the deposit composition as well as the formation mechanism. Indeed, changes in the experimental conditions may result in electrodeposition with different microstructures, compositions, phases, and magnetic properties.

The purpose of the present work is to study the effect of the plating parameters (applied potential and deposition time) on the Ni-P structure through a careful simulation of the X-ray diffraction patterns. Composition, surface morphology, microstructure, and structure of the deposits were investigated by scanning electron microscopy, energy-dispersive X-ray analysis, and X-ray diffraction. Magnetic measurements were used in combination with XRD to distinguish between phases with strong and weak magnetic properties since Ni-P deposits form different phases.

2 Materials and Methods

Ni-P films were electrodeposited under potentiostatic conditions onto polished copper substrates with an exposed area of about 1 cm² and a thickness of about 60 μm. Three applied potentials (−1, −1.15, and −1.3 V) were set up in order to follow the formation mechanism of the Ni-P deposits during 10 and 20 min. Hence, six deposits named samples A (−1 V, 10 min), B (−1.15 V, 10 min), C (−1.3 V, 10 min), D (−1 V, 20 min), E (−1.15 V, 20 min), and F (−1.3 V, 20 min) were prepared. The experiments were performed using an electrochemical technique by means of the three-electrode potentiostat/galvanostat PARSTAT 2253. The substrates were mechanically polished with SiC emery paper and subsequently treated in order to remove the

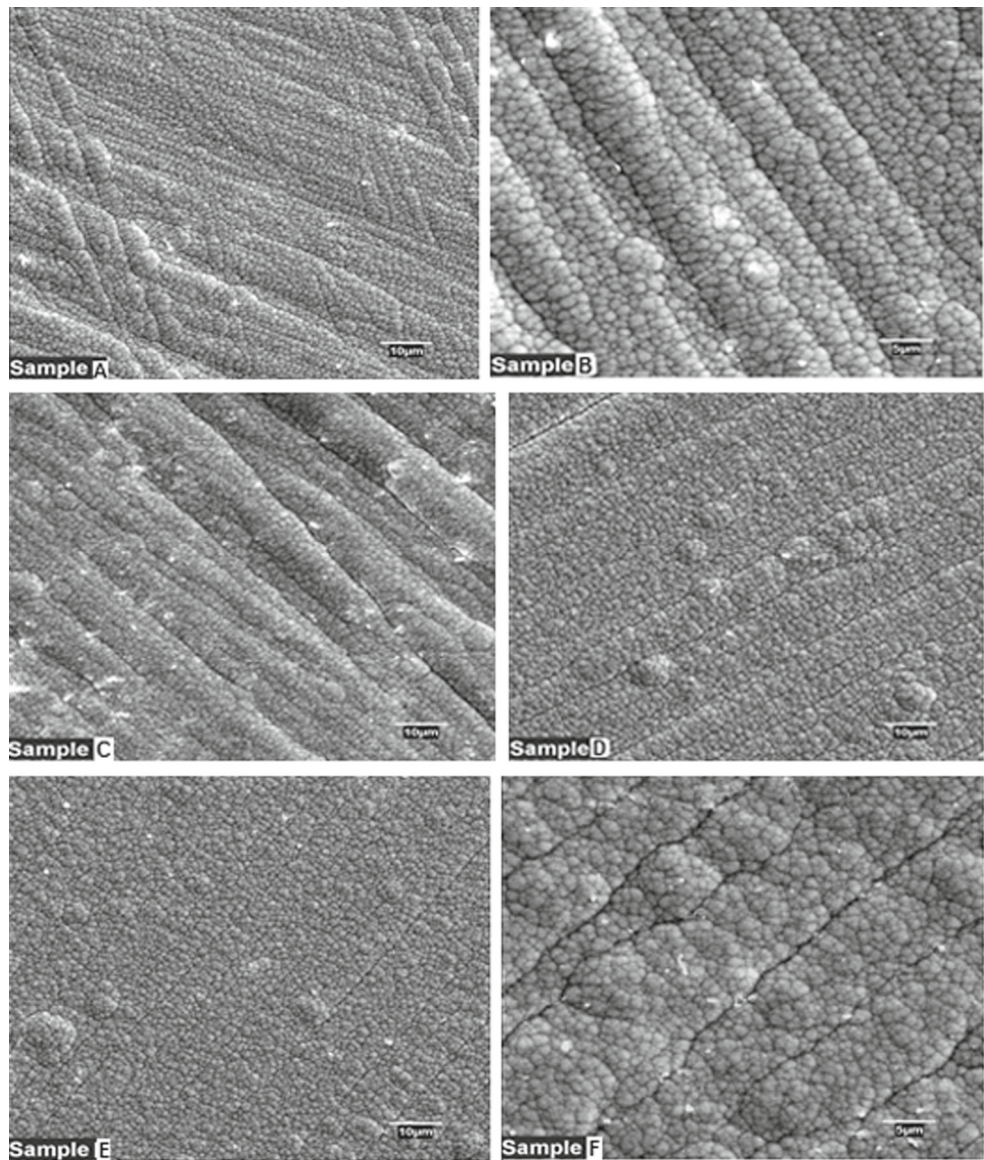
impurities by two successive baths—acetone (99.5 %) then ethanol (95 %)—and finally rinsed in deionized water. The pre-cleaned copper substrates were used as working electrodes. A nickel foil was used as a counter electrode and saturated calomel KCl (SCE) as a reference electrode. The distance between the anode and the cathode was maintained at 4 cm in order to ensure uniform deposition. The operating temperature was 70 ± 2 °C and the bath pH was maintained at 3–4. The plating parameters such as the bath composition and the operating parameters are summarized in Table 1.

Microstructural analysis was performed on the surface and cross section of the Ni-P deposits by scanning electron microscopy (SEM, Zeiss DSM-960A) operating at a voltage of 20 kV with energy-dispersive X-ray spectroscopy (EDX). Structural changes of the deposited coatings as a function of the applied potential and deposition time were studied by X-ray diffraction (XRD) using a PanAnalytical powder diffractometer in Bragg Brentano ($\theta - 2\theta$) geometry in the range 20°–120° with a step size of 0.02°, a counting time of 10 s/step, and a Cu-K α radiation ($\lambda_{\text{Cu}} = 0.154056$ nm). The XRD profiles were analyzed through the Maud program [18] which is based on the Rietveld method [19]. Instrumental parameters, like 2θ correction, peak asymmetry, and peak broadening parameters (U , V , W) of a LaB₆ standard sample, assumed to have no size and strain broadening, have been used as fitting parameters in the software. The quality of the refinement is estimated from the various numerical criteria of fit, namely the weighed residual factor (R_{wp}), the Bragg factor (R_{b}), the expected factor (R_{exp}), and the goodness of fit (Gof) obtained from the analysis procedure. Magnetic measurements were carried out using a vibrating sample magnetometer (VSM, MicroSense). The measurements were conducted on the as-deposited samples by applying an external field of 20 kOe in the plane and out of the plane.

Table 1 Composition and operating conditions used for Ni-P deposits

Bath composition	Concentration
Nickel sulfatehexahydrate (NiSO ₄ · 6H ₂ O)	0.2 M
Sodium hypophosphite (NaH ₂ PO ₂ · H ₂ O)	0.10 M
Boric acid H ₃ BO ₃	0.005 M
Saccharin (C ₇ H ₅ NO ₃ S)	0.005 M
Sodium chloride (NaCl)	0.7 M
Operating conditions	
Parameters	Value
pH	3–4
Temperature	70 ± 2 °C
Potential	−1.3, −1.15, and −1 V
Deposition time	10 and 20 min

Fig. 1 SEM surface morphologies of the Ni-P deposits



3 Results and Discussion

Representative surface morphologies of the Ni-P coatings are displayed in Fig. 1. The deposits are dense, regular, and uniform with nearly-spherical-shaped fine nodules and exhibit some cracks and a smooth surface. The deposits have a cauliflower morphology whereby small nodules agglomerate to form clusters or larger nodules. This can be due to a slow nucleation rate and rapid grain growth. The surface morphology is strongly dependent on the characteristics of the electroless nickel plating solution [20]. The EDX analysis reveals small variation of P content from 8.64 to 12.2 at.% (Table 2). The size distribution of the nodules is relatively narrow with a large quantity (69–82 %) of fine nodules below 1 μm (Fig. 2). The average size of nodules varies between 0.7 and 1 μm .

Cross section microstructures along the thickness direction of Ni-P films are shown in Fig. 3. Contrary to the surface morphology, the films are irregular and non-uniform

Table 2 Phosphorous content at the surface and the cross section of the deposits

Sample	Time (min)	Potential (V)	P_{surface} (at.%)	Ni (at.%)	$P_{\text{cross section}}$ (at.%)	Ni (at.%)
A		-1	11.9	88.1	5.8	84.2
B	10	-1.15	11.1	88.9	6.7	93.3
C		-1.3	08.6	91.4	8.6	91.4
D		-1	10.5	89.5	4.1	95.9
E	20	-1.15	12.2	87.8	5.3	94.7
F		-1.3	10.9	89.1	5.1	94.9

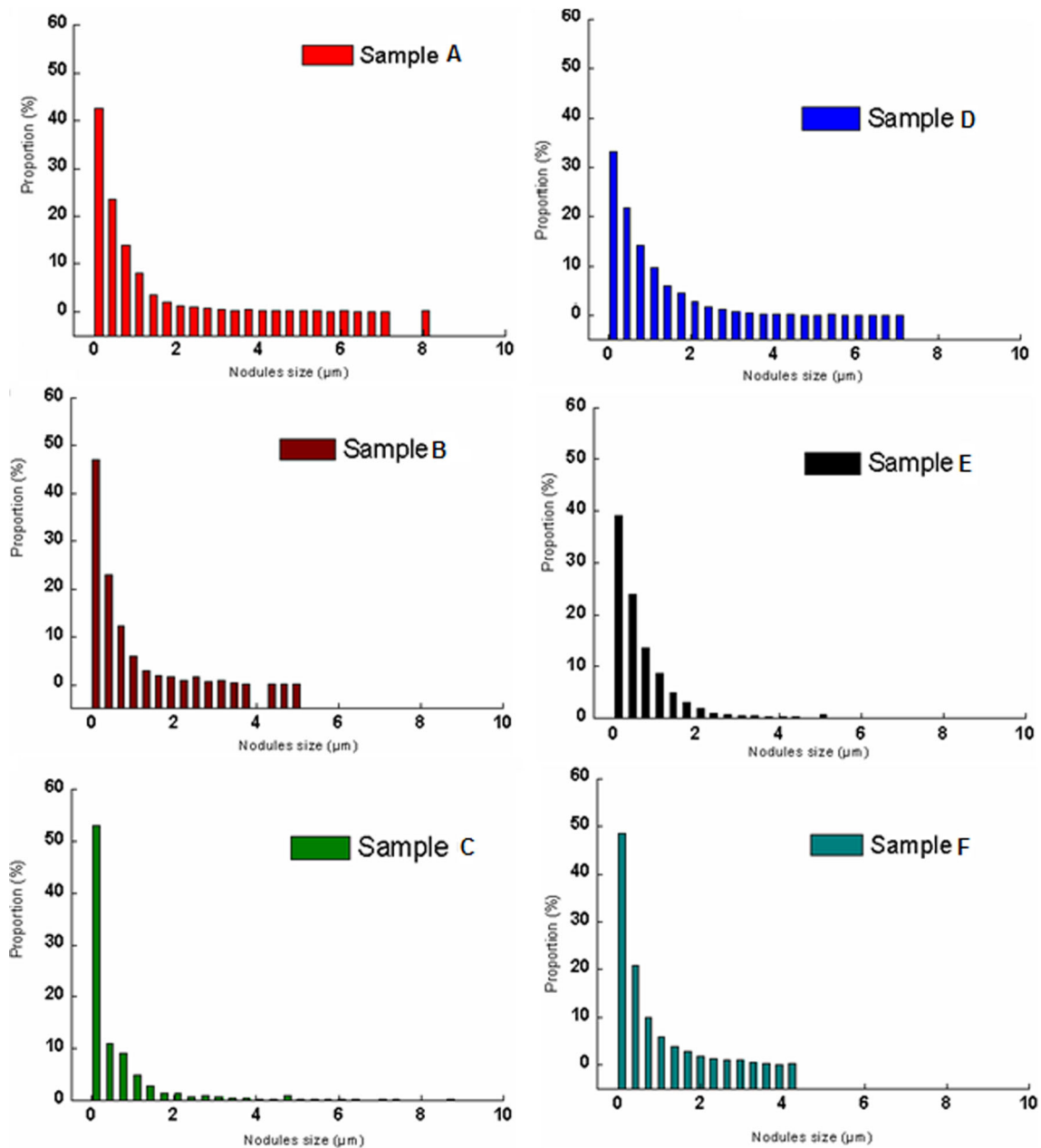


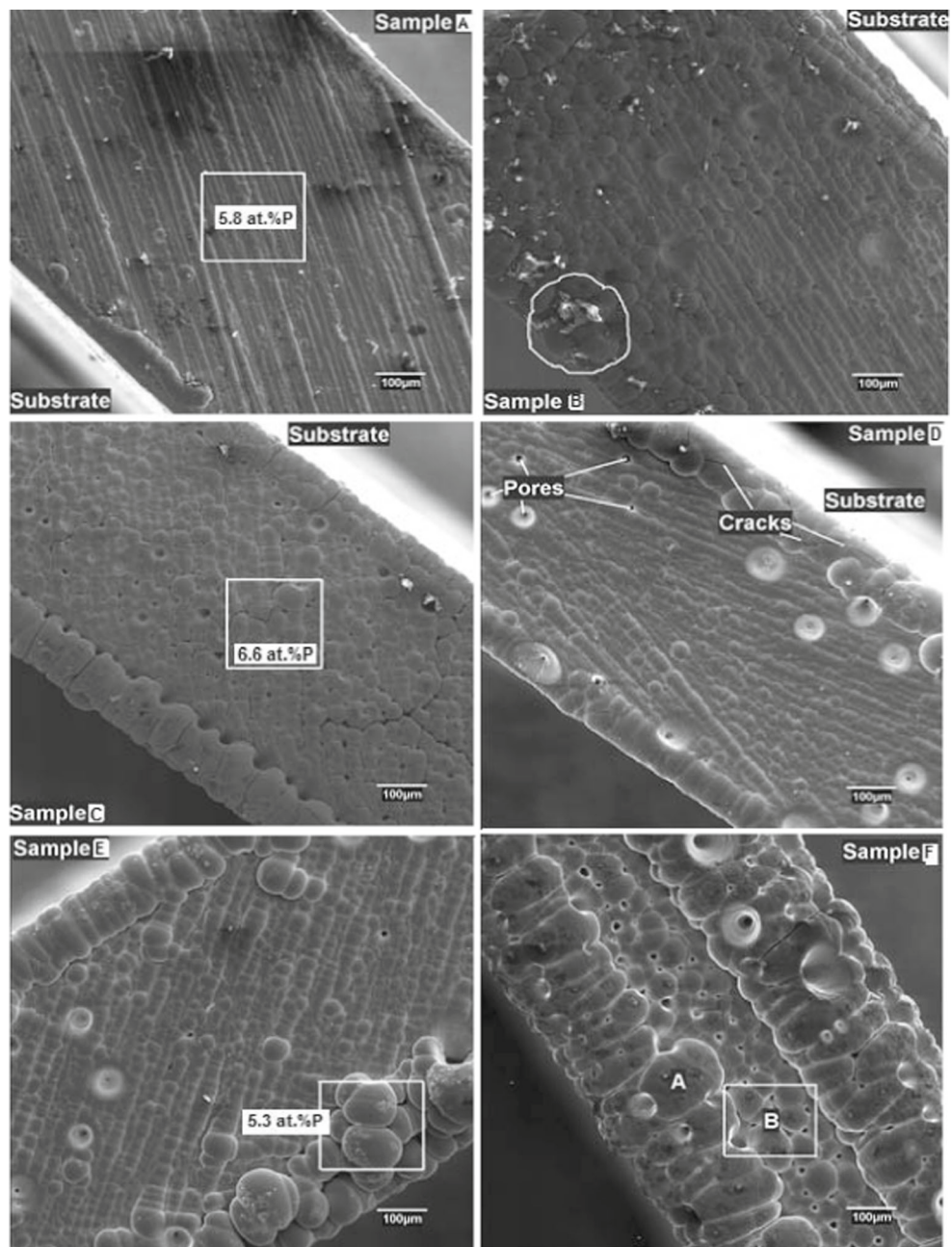
Fig. 2 Nodule size distribution of Ni-P deposits deduced from SEM surface images

and display some cracks and pores as well as different grain shapes and sizes. Sample A exhibits different morphologies characterized by a lamellar structure that can be ascribed to the variation in the composition with thickness from the surface to the deposit/substrate interface. In general, the lamellar structure can be seen in alkaline baths [21, 22] which are more pH dependent than acidic baths. The formation of laminates might be related to the fluctuation in the pH of the plating solution adjacent to the deposit surface. This fluctuation results in variation of the P content as confirmed by the EDX analysis. Indeed, the P content changes from exterior to interior (Table 2). Along

the thickness direction, the composition is low P content (4–6.6 at.%), while that of the surface is medium P (8.6–12.2 at.%). The deposits are coarser and agglomerate at the periphery to form clusters. This behavior might be due to a slower nucleation rate and faster grain growth. The cracks can be related to residual stresses developed as a result of the finer-grained and denser deposits.

Figure 4 displays the XRD patterns of the Ni-P films. The broadening of the Ni diffraction peaks can be related to the grain size refinement and the formation of the Ni(P) solid solution as well as the amorphous phase. The patterns are nearly similar except that of sample A. This result is

Fig. 3 Cross-section morphologies along the thickness direction of Ni-P films



in good agreement with the SEM observation. Hence, the XRD patterns were computer fitted using three phases: two Ni(P) solid solutions and Ni₂P phosphide for sample A, and two Ni(P) solid solutions in addition to an amorphous structure for the other samples. Only the Rietveld refinements of the XRD patterns of samples A and C are shown in Fig. 5. The formation of the Ni(P) solid solution with different compositions may be due to the competition between atoms to form a substitutional solid solution by replacing some Ni atoms by P ones. In fact, P dissolves substitutionally into the metal lattice to form a metastable solid solution. According to the very low solubility of P into the Ni

lattice on the one hand and because the Ni-P deposits contain more of the alloying element (P) than the host face-centered cubic (fcc)-Ni matrix can dissolve on the other hand, then the surplus must separate out to give regions that have a high concentration of P as well as chemical compounds such as Ni₂P phosphide. This might explain the presence of two Ni(P) solid solutions with different P concentrations, different lattice parameters, and different crystallite sizes. Since the Ni(P) solid solutions have the same structure, the boundary is still coherent but has some strain (and more energy) associated with it [23]. The rapid diffusion of P into the Ni lattice can be ascribed to the

Fig. 4 XRD patterns of the Ni-P films as a function of plating conditions (potential and time)

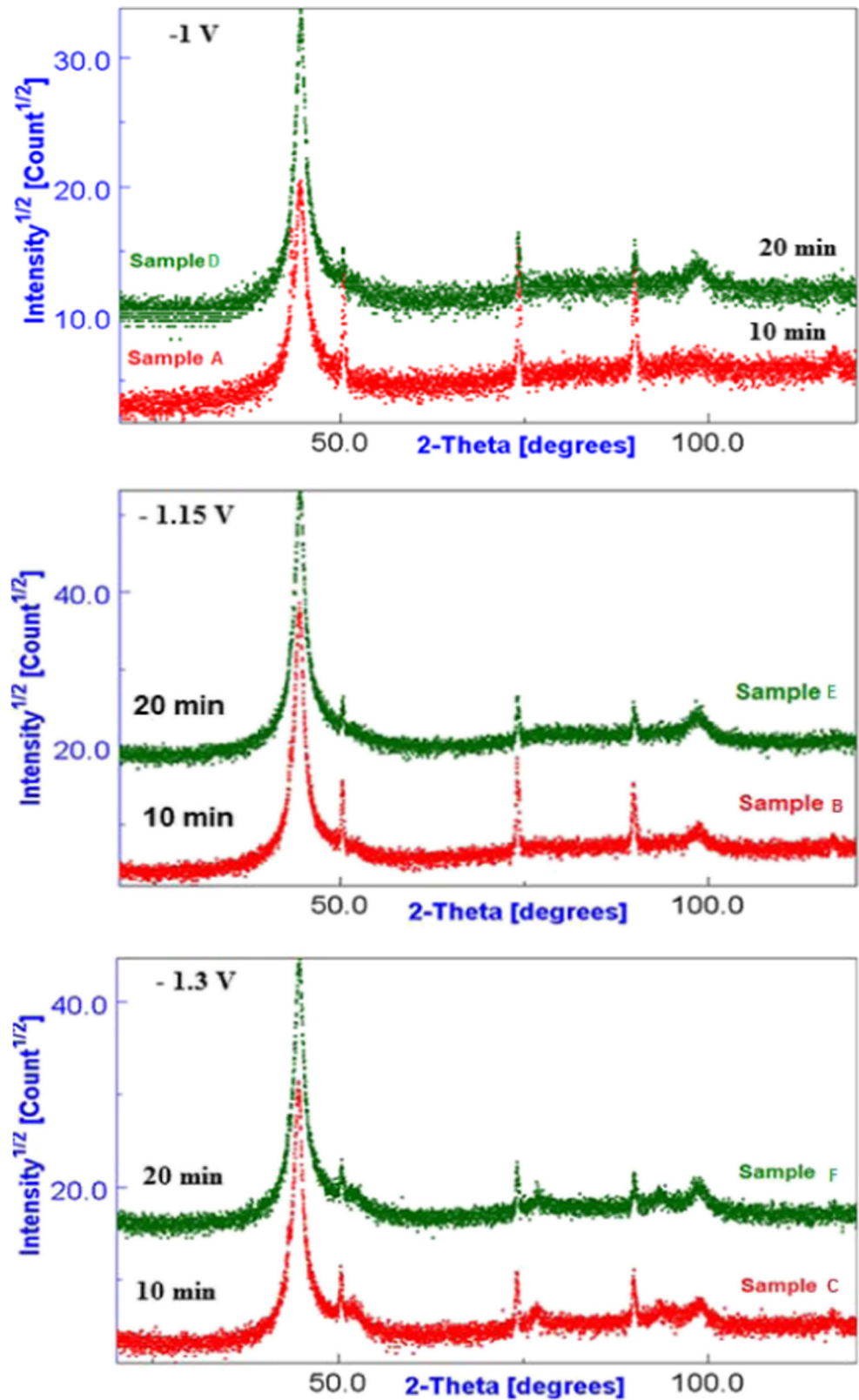
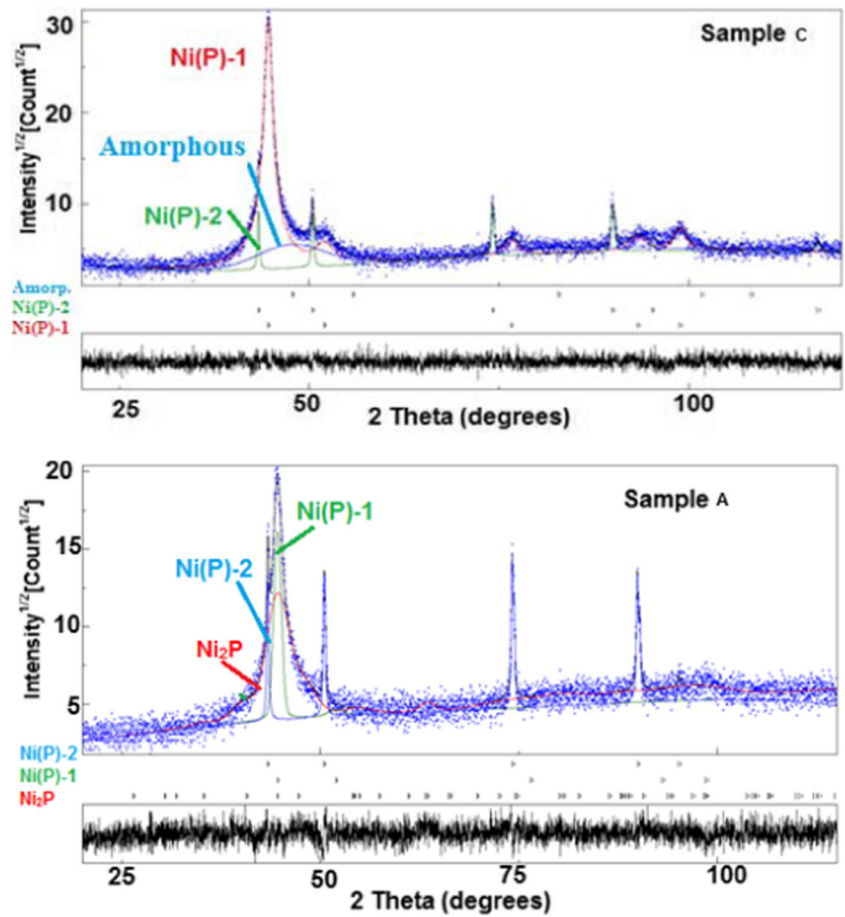


Fig. 5 Rietveld refinement of the XRD patterns of samples A and C. Experimental (dots) and calculated (full line) patterns are shown. Difference between experimental and calculated patterns is given below



enthalpy of mixing which is strongly negative ($\Delta H_{Ni-P} = -26$ kJ/mol). Ni_2P adopts the hexagonal Fe_2P structure with lattice parameters $a = b = 0.5859$ nm and $c = 0.3382$ nm. The structure of the metal-rich phosphide is based on trigonal prisms, which can well accommodate the relatively large phosphorus atoms. The deduced structural and microstructural parameters from the Rietveld refinement are summarized in Tables 3 and 4.

According to the phase diagram of the Ni-P system, the equilibrium phases are Ni and Ni_3P for a phosphorous content up to 25 at.% and the maximum solid solubility of P in Ni is 0.32 at.% at the eutectic temperature (870 °C). Therefore, P is practically insoluble in the Ni lattice at the deposition temperature (70 °C). As a result, the formation of an equilibrium Ni(P) solid solution is not thermodynamically favored at this temperature. Consequently, the

Table 3 Structural and microstructural parameters as a function of applied potential for 10 min

Potential (V)	Phases	$\langle L \rangle$ (nm) (± 1)	a (nm) ($\pm 10^{-4}$)	Δa (%)	c (nm) ($\pm 10^{-4}$)
-1.3	Ni(P)-1	10	0.3515	-0.37	-
	Ni(P)-2	93	0.3617	2.52	-
	Amorphous	-	-	-	-
-1.15	Ni(P)-1	09.6	0.3521	-0.20	-
	Ni(P)-2	95	0.3617	2.52	-
	Amorphous	-	-	-	-
-1	Ni(P)-1	98	0.3524	-0.11	-
	Ni(P)-2	100	0.3618	2.55	-
	Ni_2P	96	0.5884	0.42	0.3382

Table 4 Structural and microstructural parameters as a function of applied potential for 20 min

Potential (V)	Phases	$\langle L \rangle$ (nm) (± 1)	a (nm) ($\pm 10^{-4}$)	Δa (%)
-1.3	Ni(P)-1	10	0.3526	-0.05
	Ni(P)-2	51	0.3631	2.91
	Amorphous	-	-	-
-1.15	Ni(P)-1	9.6	0.3527	-0.03
	Ni(P)-2	80	0.3623	2.69
	Amorphous	-	-	-
-1	Ni(P)-1	9.8	0.3532	0.11
	Ni(P)-2	89	0.3631	2.91
	Amorphous	-	-	-

structure of the Ni-P deposits is far from the thermodynamic equilibrium.

Phosphorous can be co-deposited with nickel from solutions containing both Ni and P ions. Electrolytic formation of nickel takes place in the fcc structure and the co-deposition of phosphorous occurs in the octahedral interstitial sites. The amount of P influences the Ni-P alloy structure which undergoes transitions from crystalline to NC and eventually becomes amorphous with increasing P content owing to P atoms disturbing the regular arrangement of Ni atoms [24]. During the co-deposition process, the reduction of Ni^{+2} ions at an active center on the cathode surface is followed by the surface diffusion of the Ni adatom to a suitable crystal lattice site. By increasing the P content in the deposit, the rate of fresh nucleus formation becomes higher than that of growth of an existing crystal nucleus leading to a deposit crystallite size refinement. Therefore, nucleus growth ceases at a critical P content, giving rise to the formation of an amorphous structure having short-range

order over a few atomic distances. Mahalingam et al. have obtained a polycrystalline fcc structure at lower P concentrations (<13.5 at.%) which transformed into an amorphous structure with increasing P content in the deposit [25]. It is generally accepted that low-P alloys are supersaturated NC Ni(P) solid solution, high-P alloys are fully amorphous, while medium-P alloys are a mixture of amorphous and NC structures.

Figure 6 shows the relative proportion of the Ni(P) solid solutions as a function of applied potential for 10 and 20 min. The main component is the low-P-content Ni(P)-1 solid solution. The amorphous fraction reaches a maximum value of about 26 % for sample D. Nevertheless, for a deposition time of 10 min, the amorphous fraction increases slightly from 8 % for sample C to 13 % for sample B. Accordingly, coatings with a phosphorous content of about 10–12 at.% can be regarded as partially amorphous, whereas those with approximately 8 at.% P can be considered NC.

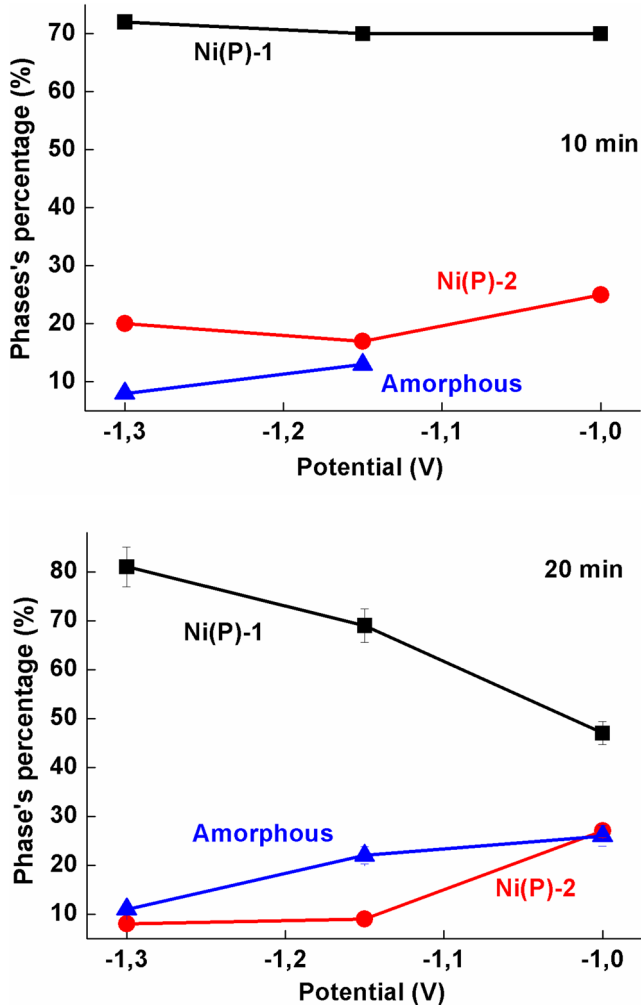


Fig. 6 Evolution of the phases' fraction as a function of the applied potential during 10 and 20 min

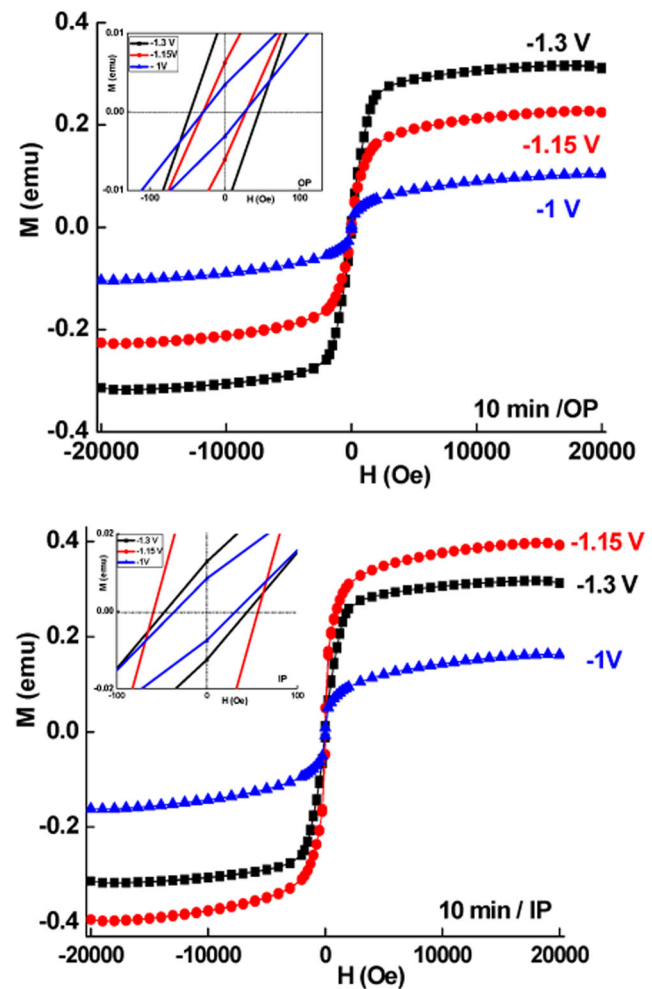


Fig. 7 Magnetic hysteresis curves of the films deposited for 10 min in two applied field directions. The inset is the zoom-in information at low field

The average crystallite size of the Ni(P)–1 solid solution increases from 10 nm at -1.3 V to about 98 nm at -1 V for a deposition time of 10 min, while it remains nearly constant (~ 10 nm) for 20 min (Table 3). In the case of the Ni(P)–2 solid solution, the average crystallite size varies slightly from 93 to 100 nm for a deposition time of 10 min and decreases from 89 nm at -1 V to 51 nm at -1.3 V for a deposition time of 20 min (Table 4). The supersaturating of the Ni structure by P can inhibit the growth of Ni crystallites whose size becomes smaller until complete formation of the solid solution. The significant grain refinement can be due to the grain refiner such as saccharin which is used in the composition bath to retard the grain growth of deposits [1].

Phosphorous content is essential in establishing the structure of the Ni-P matrix. The lattice parameters of the NC Ni(P) solid solutions (Tables 3 and 4) deviate weakly from the equilibrium value of the perfect Ni crystal $a_0 = 0.3528$

nm. This might be related to the size closeness of the host Ni ($r_{Ni} = 0.135$ nm) and the dissolved P ($r_P = 0.128$ nm) atoms. In fact, P simply replaces some of the host ones to give a substitutional fcc Ni(P) solid solution with a lattice parameter merely identical to that of the fcc Ni structure. The relative deviation $\Delta a = (a - a_0)/a_0$ of the lattice parameter of the Ni(P)–1 solid solution varies between -0.37 and -0.03 %, while that of the Ni(P)–2 is much greater (2.52–2.91 %). Such relative deviations can be ascribed to the variation of the P content in the Ni lattice. Hence, the Ni(P)–2 structure can be considered as a supersaturate solid solution. Indeed, if we suppose that Vegard's law [26] is valid in the case of the Ni(P) solid solution, the P concentration which is calculated from the measured lattice parameter is found to be 0.08–1.05 at.% P for Ni(P)–1 and 7.2–8.31 at.% P for Ni(P)–2. Therefore, the Ni(P)–1 can be considered as an equilibrium solid solution where the solubility limit of P in the Ni lattice is enhanced to 1 at.% because of the lattice strained in nanocrystallines. However, the Ni(P)–2 structure can be considered as a supersaturated solid solution since the P content is about 22.5–25 times the equilibrium solubility of P into the Ni lattice. The P content in the Ni(P) solution nanophase crystallized from an amorphous $Ni_{80}P_{20}$ alloy was found to be 10–15 times the equilibrium solubility [27]. In spite of the fact that the solid solubility of P in Ni is negligible at lower temperature, it is possible to produce a highly supersaturated Ni(P) solid solution with electrodeposition since the P solubility in the NC Ni solution may be considerably enhanced. It has been reported that the amount of co-deposited P with Ni solid solution in the electrodeposited Ni-P alloys is as high as 12 at.% [28]. In the electrodeposited NC Ni(P) with grain size in the range of 5–10 nm, the P concentration was approximately 1.2 wt% [29]. The large volume fraction of grain boundaries and/or internal interfaces in the NC alloys provides a great potential for the solubility improvement. The enhancement in the solubility during grain size

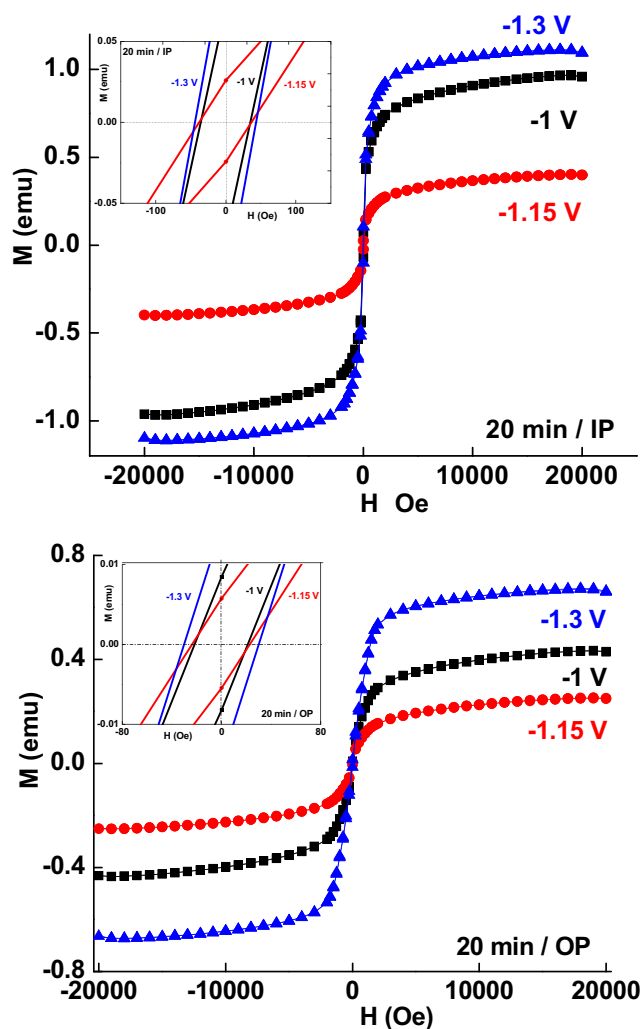


Fig. 8 Magnetic hysteresis curves of the films deposited for 20 min, in two applied field directions. The inset is the zoom-in information at low field

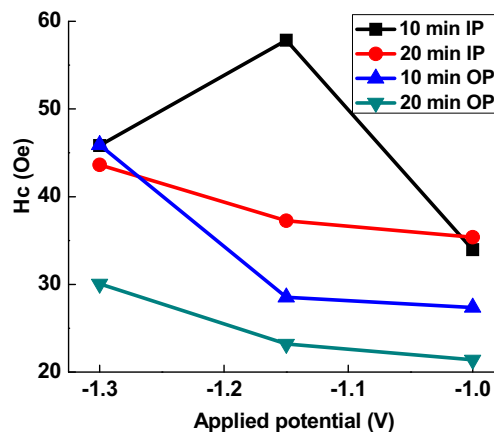


Fig. 9 Variation of coercivity as a function of the applied potential

refinement can be ascribed to the increase of Gibbs free energy resulting from the introduction of high-energy grain boundaries.

The hysteresis loops of NiP samples are presented in Figs. 7 and 8 as a function of the applied potential for 10- and 20-min deposition times, respectively. The insets are the zoom-in information at low fields. One observes that the Ni-P films are magnetic and the hysteresis loops are extremely thin for all samples. Since the amorphous Ni-P alloy and all other Ni-P compounds are paramagnetic, the magnetic properties of the nanocrystalline Ni-P films are due to the presence of bcc Ni(P)-1 and Ni(P)-2 solid solutions.

The shape of a hysteresis curve is determined partly by the domain state which can be distinguished by the squareness ratio M_r/M_s and the coercivity, H_c .

Depending on the morphology and microstructure of samples as well as the direction of the external applied field, significant differences in the coercivity field values are noticed. In fact, the coercivity decreases with increasing the applied potential for all samples except that of sample B when the applied field is parallel to the film plane where H_c reaches a maximum value of about 57.85 Oe (Fig. 9). The soft magnetic character of the deposits can be related to the reduction of the size of coherently diffracting domains.

Figure 10 represents the variation of the squareness ratio M_r/M_s as a function of the applied potential. One observes that the M_r/M_s ratio is plating condition (time and potential) dependent for the in-plane field direction. However, it is nearly constant for the out-of-plane field direction. The reduction of the M_r/M_s ratio can be linked to the amorphization process that leads to a reduction in magnetic anisotropy. From the value of the M_r/M_s ratio, it is possible to differentiate between single-domain (SD) and non-SD particles. Hence, the M_r/M_s ratio values which are in the range of 0.019–0.123 are much lower than the expected value for a random distribution of the easy axis for particles with uniaxial anisotropy (0.5) [30]. For sample B, the M_r/M_s value corresponds to a pseudo-single domain (PSD), while those

of the other samples (< 0.1) correspond to a multidomain (MD) [31]. For the latter, the change of the magnetization can be accomplished by the translation of the domain wall, an energetically easy process, in relatively low fields.

4 Conclusions

Ni-P coatings were prepared by electrodeposition using different plating conditions. The phosphorous content is medium (8.64–12.21 at.%) at the surface and low (4.1–6.59 at.%) across the depth. The deposits exhibit either a composite structure or a mixture of the NC Ni₂P (5 %) compound and Ni(P)-1 and Ni(P)-2 solid solutions. The P content in the Ni(P)-2 nanophase is found to be about 22.5 to 25 times that of the equilibrium solid solubility. All samples exhibit a soft magnetic character with coercivity lower than 58 Oe. The M_r/M_s values (< 0.1) correspond to MD for all samples except that of sample B which corresponds to PSD.

Acknowledgments This work was supported by the DGRSDT/PNR project no. 27/53, 2011 (MESRS) Algeria.

References

1. Tebbakh, S., Messaoudi, Y., Azizi, A., Fenineche, N.E., Schmerber, G., Dinia, A.: *Trans. IMF* **93**, 196 (2015)
2. Kim, D., Park, D.-Y., Yoo, B.Y., Sumodjo, P.T.A., Myung, N.V.: *Electrochim. Acta* **48**, 819 (2003)
3. Jothi, S., Jianshe, L., Wei, S.: *J. Alloys Compds.* **571**, 183 (2013)
4. Mallory, G.O., Hajdu, J.: *Electroless plating: fundamental and applications*. AESF, USA (1990)
5. Jeong, D.H., Erb, U., Aust, K.T., Palumbo, G.: *Scripta Mater.* **48**, 1067 (2003)
6. Daly, B.P., Barry, F.J.: *Int. Mater. Rev.* **48**, 326 (2003)
7. Haidu, J.: *Trans. Inst. Met. Finish* **75**, B7 (1997)
8. Stepiewski, W., Dziedzic, A., Borecki, J., Koziol, G., Serzysko, T.: *Circuit World* **40**, 7 (2014)
9. Clark, P., Wang, X., Oyama, S.T.: *J. Catal.* **207**, 256 (2002)
10. Jiaqiang, G., Yating, W., Lei, L., Bin, S., Wenbin, H.: *Mater. Lett.* **59**, 1665 (2005)
11. Zhang, L., Jin, Y.B., Wang, Z., Yang, Y.X., Jianyu, Q.: *Appl. Surf. Sci.* **255**, 1686 (2008)
12. Tjong, S.C., Chen, H.: *Mat. Sci. Eng.* **R45**, 1 (2004)
13. Bonino, J.-P.: *J. Appl. Elect.* **27**, 1193 (1997)
14. Lin, C.S., Lee, C.Y., Chen, F.J., Li, W.C.: *J. Electrochem. Soc.* **152**, C370 (2005)
15. Kumar, P.S., Nair, P.K.J.: *Mater. Process. Technol.* **56**, 511 (1996)
16. Martyak, N.M.: *Chem. Mater.* **6**, 1667 (1994)
17. Brenner, A., Couch, D.E., Williams, E.K.: *J. Rees. Nat. Bar. Stand.* **44**, 109 (1950)
18. MAUD program, www.ing.unitn.it/~maud/
19. Rietveld, H.M.: *J. Appl. Cryst.* **2**, 65 (1969)
20. Chen, B.H., Hong, L., Ma, Y., Ko, T.M.: *Ind. Eng. Chem. Res.* **41**, 2668 (2002)
21. Sha, W., Murphy, C.J., Quinn, J.: *J. Alloys Compd.* **287**, L7 (1999)

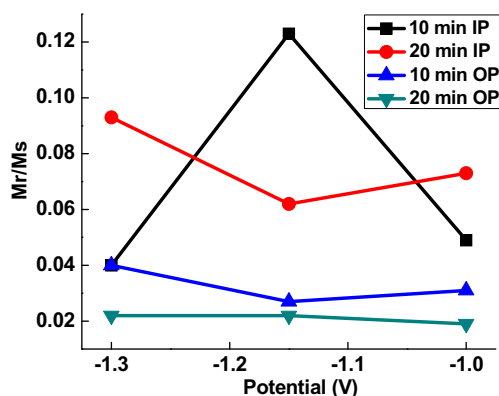


Fig. 10 Squareness ratio M_r/M_s as a function of the applied potential

22. Balaraju, J.N., Millath Jahan, S., Jain, A., Rajam, K.S.: *J. Alloys Compd.* **436**, 319 (2007)
23. Ashby, M.F., Jones, D.R.H.: *Engineering Materials 2: An introduction to microstructure, processing and design*, second ed., vol. 17. Butterworth Heinemann, Oxford (1998)
24. Luborsky, F.E.: *Amorphous Metallic Alloys*. Butterworths, London (1983)
25. Mahalingam, T., Raja, M., Thanikaikarasan, S., Sanjeeviraja, C., Velumani, S., Moon, H., Kim, Y.D.: *Materials* **58**, 800 (2007)
26. Hentschel, T.H., Isheim, D., Kirchheim, R., Müller, F., Kreye, H.: *Acta Mater.* **48**, 933 (2000)
27. Färber, B., Cadel, E., Menand, A., Schmitz, G., Kirchheim, R.: *Acta Mater.* **48**, 789 (2000)
28. Lu, K., Sui, M.L., Lück, R.: *Nano Struct. Mater.* **4**, 465 (1994)
29. Fournet, G.: *J. Phys. Radium* **14**, 374 (1953)
30. Stoner, E.C., Wohlfarth, E.P.: *R. Soc. Lond. A* **240**, 599 (1948)
31. Fallot, M.: *Ann. Phys.* **6**, 305 (1936)